

Searches for the Breaking of the Time Reversal Invariance in Polarized Epithermal Neutron Optics

H. M. Shimizu^{1,*} and on behalf of the NOPTREX Collaboration

¹*Nagoya University, Nagoya 464-8602, Japan*

(Dated: December 16, 2019)

We propose to study the breaking of the time reversal invariance (T-violation) in the spin behavior of epithermal neutrons propagating through polarized nuclear targets to search for T-odd spin correlation terms beyond the standard model with an enhanced sensitivity. The neutron absorption process is dominated by the compound nuclear process, which is observed as well-resolved narrow resonances for incident neutrons in the energy region of eV. The small energy spacing between individual resonances causes the interference of partial amplitudes in the entrance channel of compound nuclear states, which may induce energy-dependent symmetry-violating effects in case the interfering partial amplitudes have opposite parities. The small admixture of the weak interaction in the nuclear interaction have been observed as parity-violating asymmetries with the enhancement as large as 10^6 concentrated in p-wave resonances ($l = 1$). The enhancement is understood as the result of the combination of the kinematical resonance enhancement of the asymmetry visibility and the statistical mechanism of the parity-violating effect in multistep processes inside the compound nuclear states. Recently we have studied the complete decomposition of partial amplitudes in the entrance channel for ^{139}La , which exhibits about 10^6 times parity-violation enhancement at the incident neutron energy of $E_n = 0.74\text{eV}$, and found that this process has a kinematical enhancement of T-violation visibility at the same order of magnitude as the parity-violation. The statistical mechanism of T-violating effects has been studied theoretically and can be expected to enable a novel search for T-violation with a meaningful discovery potential compared with other types of new physics searches via T- or CP-violation. We will apply the optical nature of neutron propagation in nuclear polarized matters to measure the T-violating effects in the forward scattering amplitude, to which the final state interaction does not contribute. In addition, this experiment is suitable to extract the isoscalar T-violating meson-nucleon coupling, which has not been selectively measured in the search for neutron electric-dipole-moment.

This experiment requires the energy-resolved intense neutron beam in the energy range of eV, which has become available after short-pulse spallation neutron sources became operational. We have concluded that the J-PARC spallation neutron source is the best neutron source to carry out this experiment among existing and planned spallation sources. If nuclear polarized target is prepared in addition to the current situation, this experiment can be put into reality. The study of polarized lanthanum target is in progress on the basis of the feasibility study of dynamical polarization of lanthanum nuclei in lanthanum aluminate single crystal diluted with neodymium ions as paramagnetic centers.

On the basis of above situation, we propose to develop and install polarized nuclear target to the neutron facility of the J-PARC and study the neutron spin behavior in polarized nuclear target, mechanism of symmetry-violating effects in compound states, search for T-violating effects and to search for new physics beyond the standard model. Although the relation between observables and fundamental CP-violation is strongly dependent on the origin of CP-violation, we compared the sensitivity to T-violation of the proposed experiment with that of neutron electric-dipole-moment search experiments by estimating their magnitude by taking only the isoscalar coupling into account ignoring isovector and isotensor couplings. The comparison suggests that a T-violation sensitivity comparable with the neutron electric-dipole-moment search can be achieved within a few days using feasibility-proven technologies and the J-PARC spallation source with the primary proton beam power of 1, MW.

I. INTRODUCTION

The absence (so far) of evidence for new physics from new particle creation at the LHC beyond the Higgs discovery reinforces the necessity of employing the broadest possible strategy for BSM searches. It seems that we may need to infer the most likely candidate answers to

the open questions in our field not from any one experimental result but from the overall pattern of observations from many different areas of research. In combination with parallel work in searches for BSM physics at the LHC, from neutrino physics, and from many other ongoing precision Standard Model tests, T violation searches in nucleons and nuclei can make a very important contribution to the type of global picture that we need to construct from laboratory experiments, astronomical observations and theory to make further progress on the many unanswered questions of the SM.

*Corresponding author: hirohiko.shimizu@nagoya-u.jp

Another powerful motivation to search for new T, B, and L-odd interactions comes from cosmology. A. Sakharov [1] suggested that CP violation (and therefore time-reversal-invariance violation, assuming CPT invariance) along with B violation and deviation from thermal equilibrium, is an essential requirement to produce the matter-antimatter asymmetry of the universe in the Big Bang. The “easy” solution to this problem of inserting the baryon asymmetry into the Big Bang by hand as an initial condition is no longer tenable if one assumes the existence of cosmic inflation to explain the space-like angular scales of correlated fluctuations in the temperature of the microwave background. Under inflation, even if the baryon number of the universe started somehow with some nonzero value, the inflation very quickly drives the baryon to photon ratio to essentially zero at very early times, and then Sakharov’s argument applies again for later times after inflation. Within this cosmological framework, the fascinating question of the microscopic origin of the observed dominance of matter over antimatter in the universe becomes a scientific question susceptible to quantitative analysis.

We notice that searches for new sources of T, B, and L violation using nucleons and nuclei are also important because they can make an essential contribution to the broader set of clues on BSM physics that we hope to get from research in other sectors. In addition, the extremely enhanced sensitivity to parity-violating effects in compound nuclear process is suggesting a new possibility to the search for T-violation.

The compound nuclear process is a resonant state with a narrow width which commonly appears at highly excited energy regions, which can be induced by the slow neutron absorption. While such nuclear process is dominated by the strong processes, large asymmetries of the resonant absorption cross section for different helicity of incident neutrons in the epithermal energy region were found for medium-heavy nuclei and intensively studied [3].

The neutron absorption process is dominated by the resonant absorption via compound nuclear states, which is observed as well-resolved narrow resonances for incident neutrons in the energy region of eV. Most of large resonances are caused by the partial wave of incident neutrons with the orbital angular momentum of 0 (s-wave). Small resonances induced by the incident neutrons with the orbital angular momentum of 1 (p-wave) are also observed among s-wave resonances. These resonances are distributed with the energy spacing of 10 – 100 eV, which is much smaller than the energy scale of direct or quasi-direct processes such as the excitation of particle-hole states in nuclei. Their width is as narrow as about 0.1 eV, which correspond to the lifetime as long as about million times of the time scale of direct process. This implies that neighboring compound nuclear states have large probability to interfere with each other and may result in the enhancement of parity-violation between s-wave and p-wave resonances consistently with the experimental facts,

in which large parity-violating asymmetries are found in p-wave resonances with neighboring s-wave sharing the same total spin as shown in Fig. 1. Figure 2 is a sum-

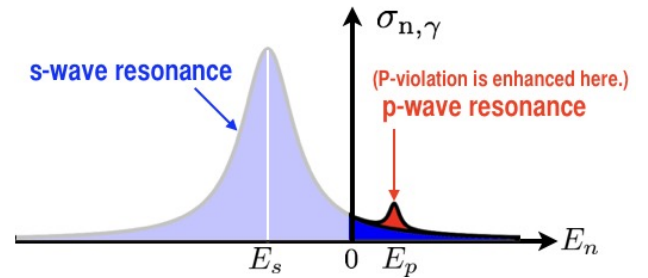


FIG. 1: Enhancement of parity violation is observed as the helicity dependence of the cross section of p-wave resonances which neighbors s-wave resonance.

mary of experimental values of large parity-violating effects, which shows that the helicity dependent asymmetry is enhanced up to 10^{-1} while that in nucleon-nucleon interaction is at the level of 10^{-7} . On the basis of the

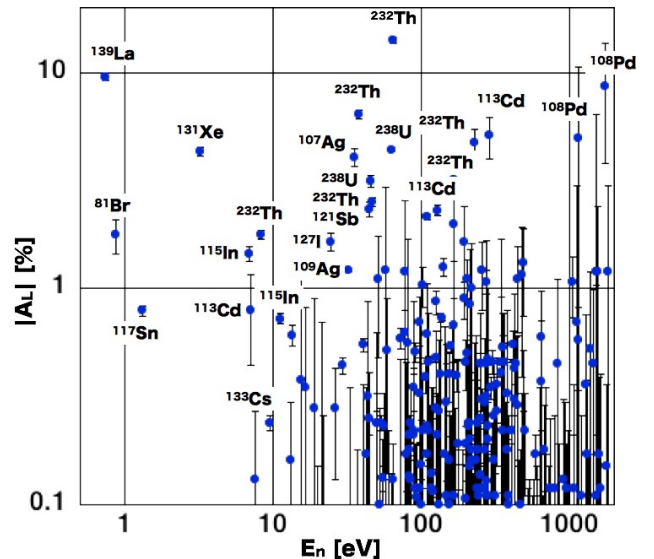


FIG. 2: Large parity violating effects. Horizontal axis is the resonance energy and the vertical axis the longitudinal asymmetry A_L , which is the ratio of the helicity dependent cross section to the resonance cross section [9].

interference between s- and p-wave amplitudes in the entrance channel, the value of A_L can be written as

$$A_L = -\frac{2xv}{|E_p - E_s|} \sqrt{\frac{\Gamma_p^n}{\Gamma_s^n}}, \quad (1)$$

where E_p and E_s are p-wave and s-wave resonance energy, Γ_s^n and Γ_p^n p-wave and s-wave neutron widths, which can be determined from the cross section measurement. The v the average value of the P-odd matrix element in the nucleon-nucleon interaction in nuclei. The x is the

fraction of partial amplitudes for p-wave neutrons with the total spin of $j = 1/2$, which cannot be determined solely from the cross section measurement. The analysis in Ref. [9] showed that the value of v can be interpreted as the averaged weak matrix element in nuclei by applying likelihood analysis with x as a randomly distributed parameter within the domain allowed by physical constraint.

The total angular momentum of incident neutron $\mathbf{j} = \mathbf{s} + \mathbf{l}$ has the value of $j = 1/2$ or $j = 3/2$. The partial neutron width for these two cases is denoted as $\Gamma_{p,1/2}^n$ and $\Gamma_{p,3/2}^n$ and x is given as $x^2 = \Gamma_{p,1/2}^n / \Gamma_p^n$. By putting $y^2 = \Gamma_{p,3/2}^n / \Gamma_p^n$, we obtain $x^2 + y^2 = 1$ from the relation $\Gamma_p^n = \Gamma_{p,1/2}^n + \Gamma_{p,3/2}^n$, which implies that we can define a real parameter ϕ as $x = \cos \phi$ and $y = \sin \phi$.

This enhancement mechanism can be generalized to other discrete symmetry for the case that two amplitudes, having opposite polarities under the symmetry operation, are connected on the boundary of the entrance channel into compound states. Reference [5] gave a quantitative estimation of the T-violation enhancement on the basis of P-violation enhancement. Below, we briefly describe the case of T-violation.

The total spin of the compound nucleus denoted by \mathbf{J} comprises of the target nuclear spin \mathbf{I} , the neutron spin \mathbf{s} and the orbital angular momentum \mathbf{l} . The state vector of the entrance channel is transformed as

$$P : |lsI\rangle \rightarrow (-1)^l |lsI\rangle, \quad (2)$$

under spatial inversion, while it is transformed as

$$T : |lsI\rangle \rightarrow (-1)^{i\pi S_y} \hat{K} |lsI\rangle, \quad (3)$$

under time reversal operation, where \hat{K} gives the complex conjugate, where $\mathbf{S} = \mathbf{s} + \mathbf{I}$ is the channel spin. This confirms that the P-violating observables arises from s-wave and p-wave amplitudes and T-violating ones from the amplitudes with different channel spins. Therefore, the kinematical enhancement of T-violation can be calculated by recombining angular momenta as

$$|(I_s)S, l, J\rangle = \sum_j \langle (I, (sl)j)J | ((I_s)S, l)J \rangle | (I, (sl)j)J \rangle, \quad (4)$$

and the corresponding forward scattering amplitude has been formulated as

$$\begin{aligned} f = & A' + P_1 H'(\hat{\mathbf{k}}_n \cdot \hat{\mathbf{I}}) + P_2 E' \left((\hat{\mathbf{k}}_n \cdot \hat{\mathbf{I}})^2 - \frac{1}{3} \right) \\ & + (\boldsymbol{\sigma}_n \cdot \hat{\mathbf{I}}) \left\{ P_1 B' + P_2 F'(\hat{\mathbf{k}}_n \cdot \hat{\mathbf{I}}) + P_3 \frac{B'_3}{3} \left((\hat{\mathbf{k}}_n \cdot \hat{\mathbf{I}})^2 - 1 \right) \right\} \\ & + (\boldsymbol{\sigma}_n \cdot \hat{\mathbf{k}}_n) \left\{ C' + P_1 K'(\hat{\mathbf{k}}_n \cdot \hat{\mathbf{I}}) - P_2 \frac{F'}{3} + P_3 \frac{2B'_3}{3} (\hat{\mathbf{k}}_n \cdot \hat{\mathbf{I}}) \right\} \\ & + (\boldsymbol{\sigma}_n \cdot (\hat{\mathbf{k}}_n \times \hat{\mathbf{I}})) (P_1 D' + P_2 G'(\hat{\mathbf{k}}_n \cdot \hat{\mathbf{I}})), \end{aligned} \quad (5)$$

where P_1 , P_2 and P_3 are the vector polarization, 2nd-rank tensor polarization and 3rd-rank tensor polarization of target nuclei and A' , B' , ... are energy dependent coefficients explicitly given in the Appendix Eq. A1 within

s-wave and p-wave interference formulated in Ref. [8]. The P-odd correlation term C' and P-odd T-odd correlation term D' in Eq. 5 can be related as

$$D' = \kappa(J) \frac{w}{v} C', \quad (6)$$

where w is the P-odd T-odd matrix element averaged in the compound nuclear state and $\kappa(J)$ is a function of ϕ given as

$$\begin{aligned} \kappa(J) = & (-1)^{J+I+\frac{3}{2}} \sqrt{2(2S+1)} \\ & \times \left(\left\{ \frac{1}{I} \frac{1}{J} \frac{1}{S} \right\} + \sqrt{2} \left\{ \frac{1}{I} \frac{1}{J} \frac{3}{S} \right\} \tan \phi \right), \end{aligned} \quad (7)$$

with $x = \cos \phi$ and $y = \sin \phi$ in Ref. [7]. The value of ϕ was recently studied for ^{139}La and the magnitude of $\kappa(J)$ is found at the order of unity [11] using the relation between the value of ϕ and the magnitude of the energy-dependent angular distribution of individual γ -rays in the vicinity of p-wave resonances [10]. Here we notice that the f contains only one unknown parameter w/v , which measures the magnitude of P-odd T-odd matrix element relative to P-odd matrix element.

The sensitivity of w/v to T-violation has been analyzed on the basis of an effective field theory as

$$\frac{w}{v} \simeq (-0.47) \left(\frac{\bar{g}_\pi^{(0)}}{h_\pi^1} + (0.26) \frac{\bar{g}_\pi^{(1)}}{h_\pi^1} \right), \quad (8)$$

at the leading order, where $\bar{g}_\pi^{(0)}$ and $\bar{g}_\pi^{(1)}$ are isoscalar and isovector T-violating meson-nucleon coupling constants, and h_π^1 is a P-violating meson exchange coupling constant, where the superscript denotes the isospin change for the process. This method was applied to interpret the experimental upper limits of nEDM and ^{199}Hg -EDM in terms of leading-order coupling constants $\bar{g}_\pi^{(0)}$ and $\bar{g}_\pi^{(1)}$ as

$$\bar{g}_\pi^{(0)} < 2.5 \times 10^{-10}, \quad \bar{g}_\pi^{(1)} < 0.5 \times 10^{-11} \quad (9)$$

in Ref. [13]. The value of h_π^1 was recently obtained from the measurement of the P-violation in $n + p \rightarrow d + \gamma$ reactions as

$$h_\pi^1 = (3.04 \pm 1.23) \times 10^{-7}, \quad (10)$$

as reported in Ref. [16] Consequently, present upper limits can be interpreted as

$$\frac{w}{v} < 3.9 \times 10^{-4}. \quad (11)$$

We notice that a suppression factor of $A^{-1/3} \sim 5$, which corresponds to $w/v < 0.8 \times 10^{-4}$, is suggested in Ref. [15].

In this proposal, we adopt Eq. 11 as the minimum success to activate a new discovery potential of the T-violation search in the forward scattering amplitude of polarized epithermal neutron optics in polarized nuclear target and propose experimental method to achieve the constraint and improve further improvement based on the progress of the proposed experiment.

In general, non-zero T-odd correlation does not always signal T-violation for scattering states, which is often referred to as the final-state-interaction. The forward scattering is the exceptional case where non-zero T-odd correlation terms directly signals T-violation. This is the remarkable advantage of the proposed experiment. However, we need to carefully design the experimental setup to suppress possible false effects carried by non-forward neutrons via single and/or multiple scatterings in the target.

II. EXPERIMENTAL PROCEDURES

We employ the optical description for the behavior of the neutron spin in the polarized nuclear target. The initial and final spinors denoted by U_i and U_f are related with the density matrix \mathfrak{S} as

$$U_f = \mathfrak{S}U_i, \quad \mathfrak{S} = e^{i\frac{2\pi\rho}{k_n}fz} \quad (12)$$

on transmission through the polarized target with the forward scattering amplitude f for the thickness of z , where ρ is the number density of target nuclei. Substi-

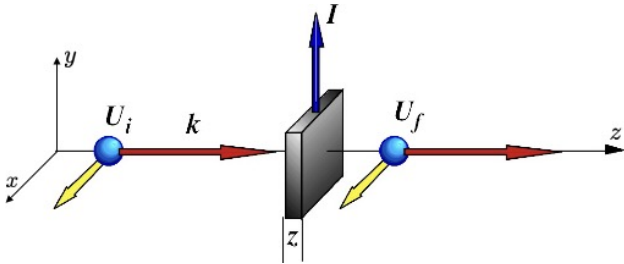


FIG. 3: Measurement of D term with polarized neutrons and polarized target.

tuting Eq. 5, we obtain

$$\mathfrak{S} = A + B(\boldsymbol{\sigma}_n \cdot \hat{\mathbf{I}}) + C(\boldsymbol{\sigma}_n \cdot \hat{\mathbf{k}}_n) + D(\boldsymbol{\sigma}_n \cdot (\hat{\mathbf{k}}_n \times \hat{\mathbf{I}})), \quad (13)$$

where

$$\begin{aligned} A &= e^{i\alpha} \cos \beta, & B &= ie^{i\alpha} \frac{\sin \beta}{\beta} \beta_B, \\ C &= ie^{i\alpha} \frac{\sin \beta}{\beta} \beta_C, & D &= ie^{i\alpha} \frac{\sin \beta}{\beta} \beta_D, \\ \alpha &= Z \left(A' + P_1 H'(\hat{\mathbf{k}}_n \cdot \hat{\mathbf{I}}) + P_2 E' \left((\hat{\mathbf{k}}_n \cdot \hat{\mathbf{I}})^2 - \frac{1}{3} \right) \right), \\ \beta_B &= Z \left(P_1 B' + P_2 F'(\hat{\mathbf{k}}_n \cdot \hat{\mathbf{I}}) + P_3 \frac{B'_3}{3} \left((\hat{\mathbf{k}}_n \cdot \hat{\mathbf{I}})^2 - 1 \right) \right), \\ \beta_C &= Z \left(C' + P_1 K'(\hat{\mathbf{k}}_n \cdot \hat{\mathbf{I}}) - P_2 \frac{F'}{3} + P_3 \frac{2B'_3}{3} (\hat{\mathbf{k}}_n \cdot \hat{\mathbf{I}}) \right), \\ \beta_D &= Z \left(P_1 D' + P_2 G'(\hat{\mathbf{k}}_n \cdot \hat{\mathbf{I}}) \right) \\ \beta &= (\beta_B^2 + \beta_C^2 + \beta_D^2)^{1/2}, & Z &= \frac{2\pi\rho}{k_n} z. \end{aligned} \quad (14)$$

According to Eq. 5 and A1, this density matrix contains the adjustable parameters, that are the nuclear polarizations P_1 , P_2 and P_3 , and the only one unknown parameter w/v . The w/v will be determined after the nuclear polarizations are determined.

Here we list some of spin-dependent observables. Following the notation in Ref. [17], the analyzing power $\mathbf{A} = \text{Tr}(\mathfrak{S}^\dagger \boldsymbol{\sigma} \mathfrak{S})$ and polarization $\mathbf{P} = \text{Tr}(\boldsymbol{\sigma} \mathfrak{S}^\dagger \mathfrak{S})$ are given as

$$\begin{aligned} A_x &= 4(\text{Re}A^*D + \text{Im}B^*C), & P_x &= 4(\text{Re}A^*D - \text{Im}B^*C), \\ A_y &= 4(\text{Re}A^*B + \text{Im}C^*D), & P_y &= 4(\text{Re}A^*B - \text{Im}C^*D), \\ A_z &= 4(\text{Re}A^*C + \text{Im}D^*B), & P_z &= 4(\text{Re}A^*C - \text{Im}D^*B), \end{aligned} \quad (15)$$

and diagonal polarization transfer coefficients defined as

$$K_{\pm i}^{\pm j} = \text{Tr} \left(\frac{1 \pm \sigma_j}{2} \mathfrak{S}^\dagger \frac{1 \pm \sigma_i}{2} \mathfrak{S} \right) \quad (16)$$

are given as

$$\begin{aligned} K_{\pm x}^{\pm x} &= |A|^2 + |D|^2 \pm 2\text{Re}A^*D, \\ K_{\mp x}^{\pm x} &= |B|^2 + |C|^2 \pm 2\text{Im}B^*C, \\ K_{\pm y}^{\pm y} &= |A|^2 + |B|^2 \pm 2\text{Re}A^*B, \\ K_{\mp y}^{\pm y} &= |C|^2 + |D|^2 \pm 2\text{Im}C^*D, \\ K_{\pm z}^{\pm z} &= |A|^2 + |C|^2 \pm 2\text{Re}A^*C, \\ K_{\mp z}^{\pm z} &= |D|^2 + |B|^2 \pm 2\text{Im}D^*B. \end{aligned} \quad (17)$$

Figure 4 shows examples of combination of observables proportional to D .

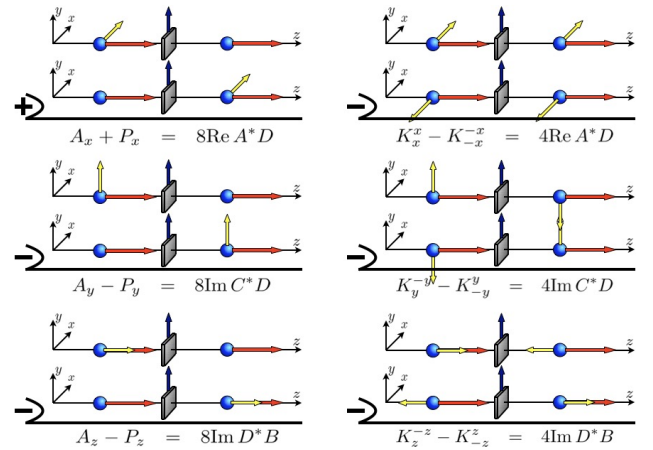


FIG. 4: Combinations of observables proportional to D .

A. Measurement of Target Nuclear Polarization

We plan to employ neutron polarizer, polarized target and spin analyzer as shown in Fig. 5 and controlling the polarizer, analyzer and spin transport between them so that we can measure the each combination of $K_{\pm i}^{\pm j}$. The

Epithermal neutrons are injected into the setup through a collimator and disk choppers, which define the beam cross section.

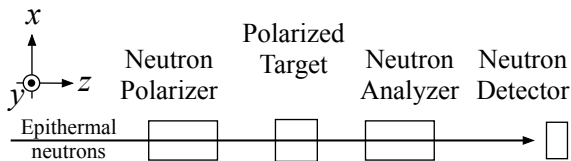


FIG. 5: Concept of experimental setup (Top view).

For determination of P_1 , K_{-x}^{+x} and/or K_{+x}^{-x} will be measured.

$$\begin{aligned} K_{-x}^{+x} &= |B|^2 + |D|^2 + 2\text{Im}D^*B \\ K_{+x}^{-x} &= |B|^2 + |D|^2 - 2\text{Im}D^*B \end{aligned} \quad (18)$$

The D is very small comparing to B . The B term consists with $P_1B' + P_2F'(\hat{\mathbf{k}}_n \cdot \hat{\mathbf{I}}) + P_3B'_3((\hat{\mathbf{k}}_n \cdot \hat{\mathbf{I}})^2 - 1)/3$. The value of K_{-x}^{+x} is oscillated as a function of neutron TOF because of the pseudomagnetic field. Although the pseudomagnetic field is compensated at the p-wave resonance energy, the oscillation occurs out of the p-wave resonance because of the neutron-energy dependence of B . The frequency of the oscillation depends on P_1B' , $P_2F'(\hat{\mathbf{k}}_n \cdot \hat{\mathbf{I}})$, and $P_3B'_3$, however, the contribution is different due to their neutron-energy dependences. For example, in the neutron energy of 1.2 eV the contribution of F' is 10^{-4} times smaller than that of B' . We can extract P_1B' by using the frequency of the oscillation of K_{-x}^{+x} out of p-wave region, then P_1 can be determined.

When we set the additional magnetic field of the compensation field at p-wave resonance region, the oscillation occurs even at p-wave resonance peak. The frequency of the oscillation include the effect from F' and B'_3 contribution, which has the magnitude of 10^{-1} of B' . We can extract $P_2(\hat{\mathbf{k}}_n \cdot \hat{\mathbf{I}}) + P_3$ from the frequency difference between near and far from p-wave resonance.

Actually P_1 and P_2 have the order of magnitude of 10^{-1} and neutron polarization is 0.7. The contrast of the oscillation may be about 0.1. The neutron counts of 10^8 is required to measure the frequency with the accuracy of 10^{-3} with the contrast of 10%. The incident neutron flux of $1.8 \times 10^7/\text{s}$ in the energy width of 0.1 eV is planned, therefore, the measurement with 10 s is enough to determine P_1 . The order of $P_2(\hat{\mathbf{k}}_n \cdot \hat{\mathbf{I}}) + P_3$ should be less than 10^{-2} , therefore, it requires 10^5 s to determine that.

In order to estimate P_3 and/or $(\hat{\mathbf{k}}_n \cdot \hat{\mathbf{I}})$, the incident beam direction is changed by scanning of the slit in front of the target. The slit with $1 \text{ cm} \times 1 \text{ cm}$ is installed and scanned vertically. The value of $(\hat{\mathbf{k}}_n \cdot \hat{\mathbf{I}})$ can be changed in the order of ± 0.002 . When we make a plot of $P_2(\hat{\mathbf{k}}_n \cdot \hat{\mathbf{I}}) + P_3$ vs $(\hat{\mathbf{k}}_n \cdot \hat{\mathbf{I}})$, the minimum value represents the P_3 and the value of $P_2(\hat{\mathbf{k}}_n \cdot \hat{\mathbf{I}})$ can be limited.

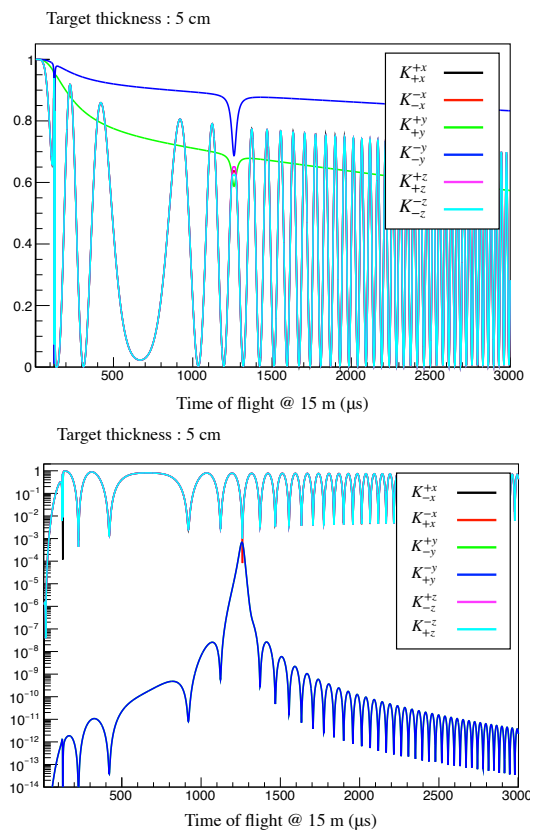


FIG. 6: Spin transfer coefficients K_{-i}^{+i} and K_{+i}^{-i} as functions of neutron TOF.

By using K_{+z}^{+z} and K_{-z}^{-z} , we can extract P_2 directly.

$$\begin{aligned} K_{+z}^{+z} &= |A|^2 + |C|^2 + 2\text{Re}A^*C \\ K_{-z}^{-z} &= |A|^2 + |C|^2 - 2\text{Re}A^*C \end{aligned} \quad (19)$$

The asymmetry of K_{+z}^{+z} and K_{-z}^{-z}

$$\frac{K_{+z}^{+z} - K_{-z}^{-z}}{K_{+z}^{+z} + K_{-z}^{-z}} \sim \frac{4\text{Re}A^*C}{|A|^2} \quad (20)$$

leads the C , which contains C' and $P_2F'/3$, not K' and B'_3 (K' and B'_3 are canceled). The P_2 value can be extracted by calculation of C' and F' . The magnitude of F' is about 10^{-1} of that of C' , and C' is 10^{-2} of the total cross section A' . For P_2 , the asymmetry with the accuracy of 10^{-4} is required. It requires about 100 s.

Finally, we can estimate the limit of $(\hat{\mathbf{k}}_n \cdot \hat{\mathbf{I}})$ by informations discussed above.

B. Interference between A and D

After determination of polarizations, the D term will be extracted by measuring the analyzing power along x -axis A_x and polarization along x -axis P_x and combine

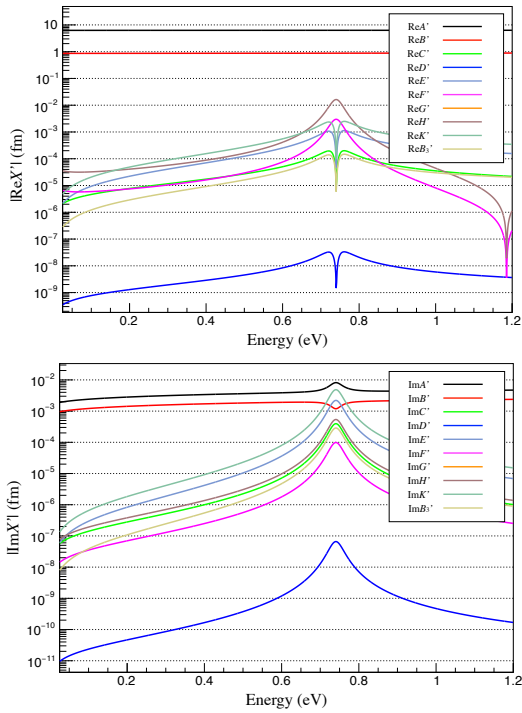


FIG. 7: Real part and imaginary part of coefficients in Eq. 5 as functions of neutron energy.

them to extract D from the relation

$$A_x + P_x = 8(\text{Re}A^* D). \quad (21)$$

The D will be redundantly determined by combining the polarization transfer coefficients K_{+x}^{+x} and K_{-x}^{-x} as

$$\frac{K_{+x}^{+x} - K_{-x}^{-x}}{K_{+x}^{+x} + K_{-x}^{-x}} \sim \frac{4\text{Re}A^* D}{|A|^2} \quad (22)$$

The systematic uncertainty from the spin control may shift the central value of the asymmetry, which will be cause the center value of the asymmetry change, however, the difference of energy dependence between A and D remains. At the p-wave resonance region $\text{Re}A^* D/|A|^2$ has the peak if D exists. We fit the asymmetry plot by Breit-Wigner function around p-wave resonance region to search T-violating effect.

C. Apparatus for the experiment

Required apparatus for this experiment is discussed below.

1. Moderator and Neutron beamline

Pulsed spallation neutron sources have the very important advantage of neutron time of flight measurement for

the neutron energy. The time width of the proton pulse and the moderator time and emission time distributions in the eV neutron energy range from the water moderators typically used in these spallation sources are narrow enough to enable one to resolve the typical widths of the p-wave resonances using neutron time of flight measurements. Furthermore one gets neutrons separated by time of flight for energies both above and especially below the resonance energy. These neutrons, which are more intense than the neutrons within the p-wave resonance width which are useful for the T violation data by more than a factor of 1000, are a very important resource for the characterization and suppression of potential systematic errors.

2. Neutron Beam Monitor

A low efficiency neutron beam monitor that is insensitive to gamma rays is needed for neutron flux normalization. We already have in hand an ion chamber using ^3He gas followed by ^4He gas of the same pressure and length. The difference signal is very insensitive to gamma rays in the beam.

3. Neutron Polarizer

We propose the use of polarized ^3He using spin-exchange optical pumping (SEOP). Polarized ^3He can be used to polarize neutrons throughout the full dynamic range of neutron energies needed for this experiment. Already the technology in use at existing neutron sources (85% ^3He polarization) is very close to the regime needed to perform this experiment. The laser power at the relevant wavelength for Rb and Rb/K optical pumping increases in ongoing R&D work for polarized ^3He use in neutron scattering, polarized targets for nuclear/particle physics experiments, and medical imaging. The neutron polarization is very uniform over the phase space of the neutron beam: this is very important for the suppression of potential sources of systematic errors. The spins of the polarized ^3He nuclei can be reversed adiabatically with nearly zero losses in polarization: this is very important for the reversal of all fields and polarizations. The on-line optical pumping is known by experience to reliably deliver a constant neutron polarization over periods of several months.

4. Polarized Neutron Spin Transport

The neutron polarization must be guided into and out of the region of the polarized nuclear target with a defined neutron polarization direction. The fields can be small on the order of 10G. This can be done with electromagnets which possess no ferromagnetic components for field generation. To check for systematics one can use

bipolar power supplies with precisely reversible currents for the external field seen by the ^3He polarizer, and the spin transport into and out of the polarized target region.

The transition of the neutron spin into the polarized target region must be handled with special care. The neutron spin must be introduced into the target region using a sharp nonadiabatic transition over a short distance. The best choice for this purpose is to pass the polarized neutrons through a superconducting magnetic shield. In addition the exact angle of the neutron spin that enters the target must be controllable in all directions. Both of these technologies has been implemented successfully already for polarized epithermal neutron scattering at the ILL in an instrument called Cryopad [ref] which performs 3D neutron polarization analysis and therefore requires the instrument to not only introduce the neutron polarization into the sample region nonadiabatically but also to be able to reorient the neutron polarization direction both before and after the target using nutation of the neutron polarization with coils.

5. Polarized ^{139}La Nuclear Target

We propose to use ^{139}La nuclei in the form of lanthanum aluminate crystals polarized using dynamic nuclear polarization. In this case the aluminum nuclei will also be polarized. This process will also generate tensor polarization as well. Using the NMR data from the experimentally achieved value of ^{139}La polarization of 47.5%, one can estimate [4–7] that the total nuclear pseudomagnetic field including the effect of the polarized aluminum is opposite to the applied magnetic field and is smaller than it would be if only from the ^{139}La . This reduces one of the most important systematic errors in the measurement from nuclear pseudomagnetic precession. We estimate that the external magnetic field needed to cancel the nuclear pseudomagnetic field inside the crystal only needs to be 0.27 T on the resonance for 100% ^{139}La polarization. This relatively small field allows us to use niobium with T_c of 8K as a superconducting shield material.

6. Forward Neutron Detector

Detectors with unit efficiency and sufficient time resolution to resolve the eV resonances well enough to see the thermal Doppler broadening of the resonance widths exist and were used at LANSCE years ago by the TRIPLE collaboration for nuclear parity violation studies. One needs a high neutron efficiency and a fast timing resolution for this detector in order to be able to resolve with the highest possible neutron time-of-flight resolution the very important p-wave resonance region as the transmission and scattering properties of the polarized target are rapidly varying in this energy region. Two of the de-

tector technologies, one based on ^{10}B liquid scintillator and another based on the detection of gamma rays from neutron capture in a $^{10}\text{B}_4\text{C}$ target followed by detection of the gamma in a NaI(Tl) scintillator array operated in current mode are both under development and will be available for this experiment.

7. Scattered Neutron Detector

The finite size of the beam for the T violation transmission experiment means that there will be some contamination of nonforward scattered neutrons which stay inside the beam envelope. These neutrons are not exactly forward scattering and therefore can cause systematic errors. At a pulsed neutron source there is a pretty way to measure these small angle scattered neutrons: almost all excitations in the target medium which scatter at small angles for incident neutrons at eV energies will scatter also at larger angles for the much more abundant neutrons at lower energies which appear later in the neutron time of flight spectrum. Therefore with a 2D neutron detector one can measure this scattered beam component which appears at later TOF and get info on the eV small angle scattering. We have in hand a 2D position sensitive neutron detector of the type usually used in small angle neutron scattering instruments.

8. Gamma Ray Detectors

Some of the polarized neutrons which enter the target will capture and make gamma rays. The asymmetries and angular distributions of these gamma rays carry useful information on the neutron polarization direction upon capture. In particular the A_{10} term in the formalism of Flambaum carries information on the entrance channel dynamics and can be useful to measure. We therefore plan to surround the polarized target with some gamma detectors.

D. Potential sources of systematic error

The systematic errors from NOPTREX are all dominated by the dynamics and interactions of the polarized neutrons in the polarized and aligned nuclear target. The dominant effect here is the spin dependence of the neutron-nucleus strong interaction which causes nuclear pseudomagnetic precession. This has already been measured for the ^{139}La and ^{27}Al nuclei and therefore one can estimate its effects in LaAlO_3 . In addition the parity violation on the resonance can also generate some systematic effects as well. Here we consider many types of potential sources of systematic errors along with an estimate of the precision with which some aspects of the apparatus need to possess for their control.

(1) *Incident Neutron Polarization Alignment.* The relative precision of the alignment of the neutron polarization direction as it enters the LaAlO_3 target should be defined at the level of about 10^{-4} . This polarization angle can be adjusted using neutron spin rotators of the same type as used in the CRYOPAD polarized neutron scattering instrument at ILL. For the measurement of this angle we can use the intense flux of slower neutrons in the beam which will spend more time in the magnetic field region and therefore get a larger rotation angle to be detected with a downstream polarization analyzer.

(2) *Uniformity of Nuclear Target Polarization.* We consider two types of target non-uniformity: large-scale polarization magnitude gradients and local small-scale variations in the polarization magnitude. The uniformity of the nuclear polarization of the target on large scales is important because, if it is nonuniform along the neutron beam direction, the parity-odd asymmetry on the ^{139}La resonance combined with the attenuation of the neutron intensity in the target can generate a neutron spin rotation that ruins the cancellation of the pseudomagnetic precession and therefore makes a systematic error. To avoid this we need a nuclear polarization uniformity. This has implications for the manner in which the microwave power is introduced into the LaAlO_3 crystal.

The spatial distribution of the ^{139}La polarization in the polarized nuclear target can also possess local nonuniformities from the different distances of the nuclei from the Nd doping centers. These centers should be reasonably uniform but this depends on the quality of crystal growth. The positive evidence for approximate spin temperature equilibrium in the previous DNP work is consistent with the spatial nonuniformities being small but this information is not direct. For direct information one can use polarized neutron imaging to perform 3D imaging of internal magnetic fields and nuclear polarization with enough spatial resolution to diagnose possible sources of systematic error from polarized target nonuniformities. These nonuniformities if present will also lead to small angle neutron scattering which can be seen in the neutron scattering detector.

(3) *Spatial Precision of Pseudomagnetic Precession Cancellation.* The nuclear pseudomagnetic field is only present where the matter is, whereas an unshielded magnetic field spreads. To prevent this from happening we need to contain the polarized target crystal tightly inside a superconducting magnetic shield to minimize the distance along the neutron beam direction where these fields are not matched. Neutron spin rotation angle for a 0.7 eV neutron in 1 cm is 66 radians/Tesla. The magnetic field penetration depth into niobium is below 100 nm. If we assume that the magnetic field is negligible after one micron penetration length into the niobium, for a 5 cm long target this gives a fractional accuracy of the cancellation of the pseudomagnetic field polarization rotation along the neutron trajectory of a few parts in 10^{-5} . The critical field for niobium superconductor is rather high: already at 4K H_{c1} is about 1.5T.

(4) *Nonforward Neutron Scattering Effects.* There are some systematic effects which can come from nonforward neutron scattering in the target. For a deviation from the exact forward scattering limit the total cross section differences are no longer exactly related to the forward scattering amplitude differences and the condition for the absence of final state effects is no longer met.

It is not possible to derive the size of these effects from first principles as they depend on the specific physics of LaAlO_3 . However we can detect the presence of processes that can lead to these systematics by using the broad distribution of neutron energies in the beam. There are about 10^4 more neutrons outside of the p-wave resonance than inside the resonance which are available to search for such scattering effects. If the inelastic neutron scattering comes from an elementary excitation of the medium (magnons for example) which is present at the resonance energy and gives a small angle scattering angle, the same excitation at the same momentum transfer Q will give a larger scattering angle for a lower incident neutron energy and therefore will be clearly visible in a downstream neutron detector outside the beam.

For elastic scattering the dominant systematic effect is from neutron diffraction in the crystal. If a neutron is diffracted into some direction then it also satisfies the diffraction condition to be scattered into the same initial direction. One can therefore get multiple scattering from two events in the crystal which sends the twice-diffracted neutron first sideways and then back into the forward direction. However these events will be delayed in neutron time of flight due to the extra distance traveled by the neutron and will appear outside the main peak in the resonance transmission data where it can be eliminated from the asymmetry analysis.

(5) *Neutron Kinetic Energy Change Upon Spin Reversal.* If the neutron changes its kinetic energy upon spin reversal it will encounter the P-wave resonance at a different neutron time of flight and therefore a false asymmetry will be generated in the transmission detector signal. The defense against this effect is to change the spin without a change in the neutron kinetic energy. There are various different ways to do this which have worked well in the past for meV and eV neutron energies. Also as long as the neutron spin reversal is applied in the low magnetic field region the change in the neutron kinetic energy is of order neV or below, which is much smaller than the 0.7 eV p-wave resonance width.

(6) *Precision of the Alignment of the Crystal.* The faces of the LaAlO_3 crystal must be parallel and oriented normal to the average neutron beam momentum. Otherwise the finite beam divergence coupled to the misalignment of the pseudomagnetic field integral along the neutron trajectory can reduce the cancellation of the pseudomagnetic field and the magnetic field.

(7) *Neutron Spin Orbit Scattering.* Electromagnetic spin-orbit scattering of the component of the neutron polarization normal to the neutron momentum will generate a left-right asymmetry which can couple to other asym-

metries to generate a systematic effect.

(8) *Polarization and Intensity Gradients in the Neutron Beam.* If the windows of the polarized ^3He neutron spin filter are not parallel then there are polarization and intensity gradients in the neutron beam. These can generate systematic errors in combination with the target pseudomagnetic precession as the beam moves through the target. If this is a problem it can be suppressed by slowly rotating the cylindrical polarized ^3He cell inside the SEOP oval about the neutron beam direction. This procedure will average out any such nonuniformities due to ^3He cell nonuniform properties.

(9) *Time Dependence of the Neutron or Nuclear Polarization or Target Magnetic Field.* If either neutron or nuclear polarization of the target magnetic field changes in time one can get a neutron transmission asymmetry upon spin reversal. As long as any of these time-dependent changes are slow they can be greatly suppressed by choosing a pattern of neutron spin reversal like $+-+--++-$ which cancels linear and quadratic components of the time dependence.

(10) *Asymmetry of Polarized Neutron Interactions in the Transmission Detector.* As the neutrons are still polarized when they are absorbed in the detector, any neutron spin-dependent interactions in the detector could cause a systematic error. The detector will be made of nonmagnetic materials and also will possess no nuclear polarization. In addition the nuclei in the detector which will be chosen to absorb the neutrons, ^{10}B , is already known to possess an extremely small parity-odd gamma asymmetry. The detector materials should also be chosen so that the circular polarization of the gammas from this process cannot scatter from the polarized electrons in a magnetized material and lead to a neutron spin-dependent detector response.

(11) *Background From Gammas in the 0.7 eV Resonance.* The total neutron width in the 0.7 eV p-wave resonance is dominated by gamma emission. If these gammas make a background in the neutron transmission detector there can be a systematic error generated. This can be reduced by shielding the detector from external gammas or by using a detector method which is insensitive to gammas, or both.

(12) *Neutron Polarization Component Along Target Polarization* In this case upon spin flips parallel and antiparallel to the target polarization, there is a transmission asymmetry from parity violation proportional to $\sigma_n \cdot \hat{I}$.

There is also a noticeable change of the kinetic energy of the neutrons as they enter the pseudomagnetic field of the polarized target. This energy change is of order $1 \mu\text{eV}$. This leads to a 2×10^{-6} shift of the neutron energy in the polarized nuclear target upon spin flip if uncompensated by any external magnetic field. The width of the 0.7 eV p-wave resonance is about 40 meV. This shift is therefore 5×10^{-5} of the p-wave resonance width.

(13) *Neutron Polarization Component Along Neutron Momentum.* In this case there is a transmission asym-

metry from parity violation proportional to $\sigma_n \cdot \hat{k}_n$.

(14) *Violations of the Adiabatic Neutron Spin Motion Upon Spin Reversal.* In this case the spin reversal is not complete and there can be unwanted components of the neutron spin passing through the polarized target which generate systematic errors. These unwanted spin components can be greatly suppressed with proper design of the neutron spin transport system.

E. Research plan

1. Measurement of $\text{Re}A^*D$

The actual design of experiment is described in this section.

The Epithermal neutrons from the poisoned moderator are injected into the setup through a collimator and disk choppers, which define the beam cross section and TOF structure. Assuming that the target area is $4 \text{ cm} \times 4 \text{ cm}$ and a neutron beam of $0.74 \text{ eV} \pm 0.05 \text{ eV}$ is used, the intensity of the neutron beam at the target position with a beam power of 1 MW is estimated using the Monte-Carlo simulation as $1.8 \times 10^7 \text{ n/s}$.

The ^3He spin filters as a neutron polarizer and an analyzer are installed before and after the polarized nuclear target of ^{130}La . The polarization direction of the neutron polarizer and analyzer based on ^3He spin filter is switched periodically. We consider the period as J-PARC MR injection timing (about every 6 s). We repeat K_{+x}^{+x} , K_{-x}^{+x} , K_{-x}^{-x} , K_{+x}^{-x} , and K_{+z}^{+z} , K_{-z}^{-z} to monitor P_1 , P_2 , P_3 and measure the D term.

There are some options to polarize the target, now we consider that the ^{139}La target is always polarized by using the dynamical nuclear polarization (DNP) technique. The target is kept in the magnetic field of 0.1 T and the temperature of 0.1 K. The microwave with the frequency of 3GHz and the power of 1 mW is irradiated onto the target while measurements. The polarization is kept to about 50% to cancel the pseudomagnetic field of the target with the external field of 0.1 T.

The magnetic field around the target must be separated between the target and beam paths just before and after the target. Neutrons with the spin of the direction of x -axis are injected adiabatically into the target through the magnetic shield. The magnetic shield is considered as a superconducting shield made with Nb. The critical magnetic field is about 0.15T.

The development of polarized target is most important and most difficult issue of this proposal. The details of the polarized target is described in next chapter.

Transmitted neutrons are detected by using a neutron detector with the counting rate of 1 GHz in maximum. We are now considering the detector as a current mode

detector, which consists of ^{10}B target and surrounding NaI gamma-ray detectors.

The gamma-ray detectors are placed surrounding the polarized target. The gamma-rays can be used to monitor the target polarization by using quantity-change or asymmetry of the (n,γ) reactions.

Scattered neutrons from the target are detected by (conventional) neutron detectors surrounding the polarized target. This enables us to study the nuclear resonance reaction precisely through the scattering amplitude.

Required measurement time is estimated. We assume the polarized target of the single crystal of LaAlO_3 , with the cross section of $4\text{ cm} \times 4\text{ cm}$ and the thickness of 2.8 cm . The value of $\text{Re}A^*D$ is 6.7×10^{-6} , which is equivalent to the limit of T-violation by neutron EDM experiments. The polarization of incident neutrons is 0.87 and the polarization of the target La is 0.4, which are achievable with today's technique. This requires the measurement time of 7.4 days.

This estimation is based on the enhancement of T-violation is the same as that of P-violation. Fadeev claimed that the enhancement of T-violation in compound nuclei should be suppressed to 1/5 of that of P-violation. If so, the required time should be extended to 185 days, which is realizable.

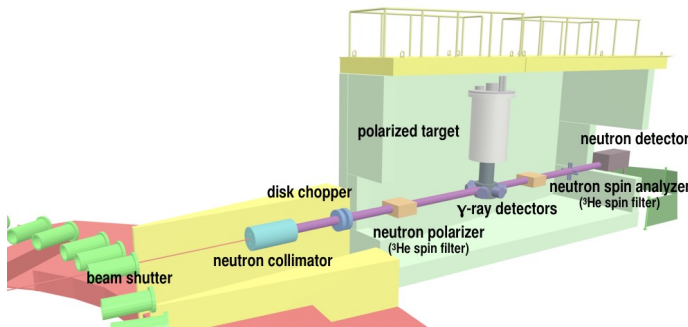


FIG. 8: 3D view of the beamline

2. Studies of Compound Nuclei and resonance reactions

In order to establish and to confirm the formalism of compound nuclei, the detailed study of the resonance reaction in compound nuclei will be performed before and while the T-violation measurement.

First, the resonance parameters, the peak energies and the widths are measured by using (n,γ) reaction. The A term can be measured with unpolarized neutrons and unpolarized target. For the precision measurement, the pulse-shape of the incident neutrons are carefully studied. The temperature of the nuclear target is controlled to estimate the doppler broadening of the peak. We have already planned the measurement of the pulse shape by using diffraction technique with perfect silicon crystal.

Although the polarization is not so high, the neutron polarizer based on ^3He is now available for epithermal neutrons. We study the C term, which is correlated to $\sigma_n \cdot \hat{k}_n$ precisely, especially its energy-dependence.

Once the polarized target is available, even though the polarization is not so high, we can start the studies of some other correlation terms, for example B term. The neutron-energy dependence is also interesting subject, which is not studied previously. We can also find F' , K' , and B'_3 terms experimentally. The details how to study each correlation term is described in Appendix.

For all studies, new dedicated beamline with epithermal neutrons is strongly recommended.

F. R&D items

1. Epithermal neutron beamline

We propose to construct a new beamline at the port BL07 which views the poisoned moderator as a compromise to accommodate this experiment.

1. Intensity of epithermal neutrons almost independent of the kind of moderators (ref. Fig. 9) J-PARC/MLF spallation neutron source has three kinds of moderators: coupled, decoupled and poisoned moderators. The time-integrated intensity $\partial\Phi/\partial E$ [$\text{cm}^{-2}\text{s}^{-1}\text{sr}^{-1}\text{eV}^{-1}$ @ 1 MW] on the moderator surface is shown in Fig. 9, which visualizes that it does not depend on the kind of moderators in epithermal region.
2. Spin control can be monitored precisely if thermal and cold neutrons are monitored simultaneously. Better time resolution is preferred.

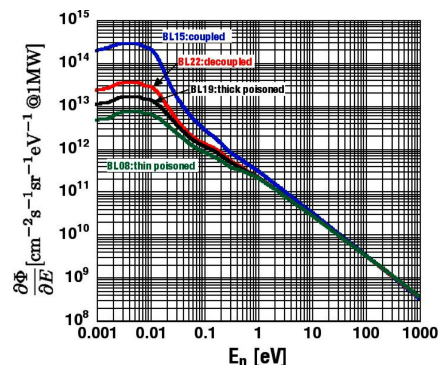


FIG. 9: Time-integrated intensity on the moderator surface $\partial\Phi/\partial E$ [$\text{cm}^{-2}\text{s}^{-1}\text{sr}^{-1}\text{eV}^{-1}$ @ 1 MW].

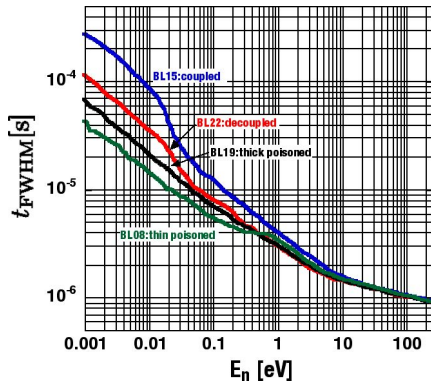


FIG. 10: Full-width at half maximum of the neutron pulse as a function of neutron energy t_{FWHM} .

2. Neutron Polarizer

In order to polarize epithermal neutrons, the candidates of the neutron polarization device are ^3He spin filter and proton spin filter. Both utilize a spin dependent cross section for neutrons to polarize neutrons. Since the ^3He spin filter is suitable for low energy neutrons less than several eV, the ^3He spin filter to polarize 0.74 eV neutrons, which is resonance energy of p-wave resonance of ^{139}La , is mainly discussed in this section.

^3He has a very large absorption cross section (10666 barn at thermal energy) for neutrons with spin antiparallel to the ^3He spin, while the absorption cross section for parallel neutrons is approximately zero. The neutron beam is polarized passing through a glass cell into which polarized ^3He is encapsulated. A figure of merit (FOM) used to describe the polarization efficiency of the ^3He spin filter is defined as

$$\text{FOM} = P^2T, \quad (23)$$

where P and T are neutron polarization and neutron transmission, respectively. As shown in Fig. 11, P , T

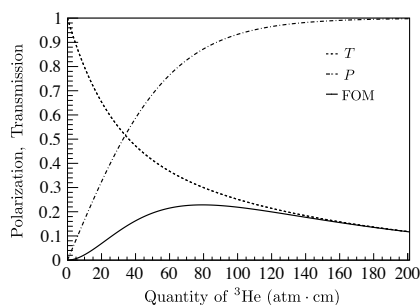


FIG. 11: The variation of the neutron polarization, transmission, and FOM as a function of the amount of ^3He for 0.74 eV neutrons, evaluated for a ^3He polarization of 70%.

and thus the FOM depends on the thickness of the ^3He ,

given by the product of the pressure of ^3He gas and the length of the ^3He spin filter. For a ^3He polarization of 70% and 0.74 eV neutrons, the FOM has a maximum at 79 atm·cm, for which $P = 87\%$ and $T = 30\%$. Therefore, we need to develop a ^3He spin filter of 79 atm·cm with 70% ^3He polarization. Since the maximum pressure of ^3He is 3.1 atm, the length of the glass cell would be 25 cm. Additionally, the radius of the glass cell should be 7 cm at least as the size of a neutron beam is $4 \times 4 \text{ cm}^2$ (a diagonal is 6.9 cm).

^3He is polarized with the Spin Optical Pumping (SEOP) method with alkali metal. Pure rubidium is enclosed with ^3He gas in the glass cell, and peripheral electrons of the Rb atoms are polarized by the circularly polarized laser. The polarization of the electrons moves to the ^3He nuclei with the hyper fine interaction, and the ^3He nuclei are polarized. Today a new technique called as 'Hybrid-SEOP' is developed to build the polarization up quickly by using spin exchange with K atoms and Rb atoms. The SEOP technique requires a high power laser with narrow bandwidth to polarize Rb.

A well-uniform magnetic field is applied to the ^3He spin filter using a solenoid and a compensation coil with a magnetic shield to maintain the ^3He polarization. The ^3He polarization relaxes by the inhomogeneity of the magnetic field, impurities inside the glass cell, collisions with other ^3He nucleus, and other effects. Especially, a clean vacuum system to encapsulate ^3He and alkali metal to the glass cell is important to fabricate ^3He which have long relaxation time.

A high power laser is also important to polarize large volume of ^3He gas. In order to polarize the large ^3He spin filter, we should irradiate the high intensity laser light (around 200W) from both sides of the ^3He spin filter to avoid attenuation of the laser light in the ^3He spin filter. Also the laser system is needed to be installed the neutron beam line to maintain high ^3He polarization in the T-violation experiment.

3. Neutron Detector

The detector used in this study is sensitive in the assumed resonance energy region, and an epithermal neutron detector that can be used in the region of approximately 1 eV is required. Assuming a full neutron beam of MLF beamline, it is desirable that the instantaneous count rate in the 1 eV region is about $100 \text{ Mcps/cm}^2 \sim 1 \text{ Gcps/cm}^2$. In addition, if estimate from statistics, in order to count about 10^{10} event in 30 days, an instantaneous count rate of 1 Mcps is required. Therefore, the performance required for the detector is at least 1 Mcps, and if possible, a neutron detector that satisfies 1 Gcps is required.

There are no fast neutron detector satisfying such an instantaneous count rate has been realized, so the following two types of detector candidates are planned and developed.

1. Current mode operation of PMT output by detecting γ rays with using ^{10}B neutron converter.
2. Development of a new high count rate neutron detector using scintillators with a short decay time constant

Currently, Kentucky University is proceeding with the design and production of 1. as the candidate detector for this research project, and the Japanese side is proceeding with the study of 2. as the backup detector.

4. Current mode detector

It is desirable that the detection efficiency is as high as possible since the measurement requires many statistics. On the other hand, the maximum instantaneous counting rate of the neutron is about $2 \times 10^8 \text{n/s/cm}^2$ in the $E_n = 1\text{eV}$ region. In such a high count rate measurement, the output signal may be continuous even when a detection element and an amplifier with a fast time constant are used. The first candidate of our transmission neutron detector is the Current Mode Detector, which is a method of reading the current of PMT output signal. Figure 24 shows the schematic view of the our Current Mode Detector, which is developed at Kentucky University. Incident neutron beam is stopped at ^{10}B converter plate and converted to 0.388 MeV γ rays. The γ rays are detected with a nearby NaI detector. The detector test is progressing at J-PARC MLF BL10 and Los Alamos Neutron Science Center.

5. Scintillation detector

In order to achieve high counting rate by photon counting the epithermal neutrons with a scintillation detector, it is required to have a fast decay time, a solid that can be segmented, and a time characteristic that allows n/ γ discrimination. Liquid scintillator containing the ^{10}B has been commonly used to detect neutrons in eV region and the candidate. The decay time of this liquid scintillator is about 4ns, very high counting rates can be achieved using this scintillator. Moreover, since γ -rays can be background for the measurement, neutron and γ -ray discrimination is also important. The discrimination can be performed by using the pulse shape difference between the neutron and the γ -ray detection. On the other hand, since the material is liquid, it is difficult to segment and it is difficult to increase the counting rate of the whole detector.

The other candidate is the ^{10}B containing plastic scintillator, and CsI(pure) scintillator with B layer. Both scintillator has the decay time of about 10 ns. Both are solid and can be segmented. The plastic scintillator is not available the n/ γ separation but there is a possibility that detection efficiency can be increased. The

CsI(pure) scintillator with B layer detector may be available n/ γ separation. The evaluation of these scintillators are proceeding.

TABLE I: Scintillator candidates

Scintillator	decay time (ns)	Neutron absorption probability at 0.75 eV 1cm thickness	n/ γ separation
B-Loaded liquid	3.2	82%	yes
CsI(pure) with Boron layer	10,36	0.8% for ^{10}B $1\mu\text{m}^t$	(yes)
Li-glass	16,49,78	93%	no
B-Loaded plastic	1.5	88%	no

A scintillator with a large light yields causes a voltage drop in the PMT in high count measurement, so it is better to use a scintillator with a small light yield.

III. POLARIZED TARGET

A. First candidate: Low field DNP

The conceptual setup around the polarized target is shown in Fig. 12. As a target material, the first candidate is a single crystal of LaAlO_3 doped with Neodymium ions and its dimension is a square of $4\text{ cm} \times 4\text{ cm}$ and a length of 5 cm . Under the assumption of 50% La polarization in the target material, the external magnetic field applied for canceling the pseudomagnetic field is 0.1 T . In order to maintain a steady strength of the magnetic field in the crystal, two superconducting magnetic shields are located at both of the front and back surfaces of the crystal and the superconducting magnet is also set inside of the shields. By ensuring that all magnetic field generated by the magnet surely comes back to the original magnet, the magnetic field inside the shields is kept in fully isolation from the outside.

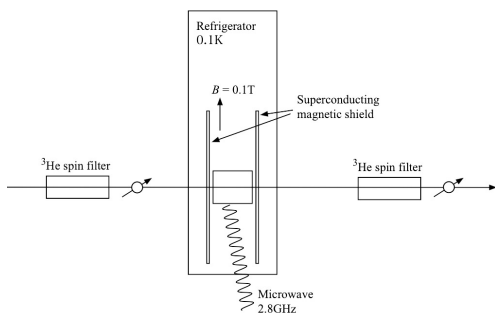


FIG. 12: Concept of setup around the polarized target

Obeying the above concept, a Helmholtz-type magnet for applying the magnetic field of 0.1 T and the magnetic shields made of Niobium are placed in the 4 K pot as shown in Fig. 13. The critical field of Niobium is about 0.2 T , which is greater than the pseudomagnetic field of 0.1 T . The 0.5 K dilution, which has a housing for the target material, can be inserted in the center of the Helmholtz magnet. The heat load of the dilution is assumed to be 1 mW at the temperature of 0.1 K .

The first plan is that the DNP is always performed during the measurement of the T-violations in the magnetic field of 0.1 T at the temperature of 0.1 K to keep the constant polarization of 50%, where the frequency of the RF pulses for irradiating the target materials is 2.8 GHz . The low field DNP is required to achieve the efficiency of 85% in the polarization transfer from electron to La nuclear spins because the thermal polarization of the electrons provided by the Neodymium elements is 58%. Although our experiences on the low field DNP are not so much, the polarization transfer in the low field is basically possible by using the Integrated Solid Effect (ISE), which is used as a general technique in the triplet DNP. In order to prevent a large loss of the RF input power and to keep the temperature of 0.1 K constant with the irradiation of

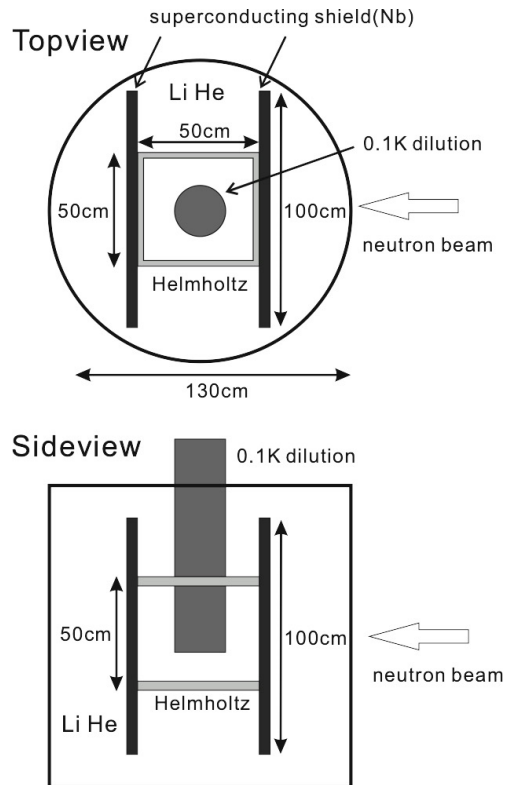


FIG. 13: Structure of the 4 K helium dewar. The Helmholtz magnet and the superconducting magnetic shields are installed inside of the 4 K dewar.

the RF pulses, we will use the rectangular RF cavity as shown in Fig. 16, which makes the target crystal fixed. The RF cavity is cooled down via a cold finger contacting to the 0.1 K mixing chamber and the target crystal is also cooled down via the RF cavity into 0.1 K . This method is very efficient, because the dominant RF power loss is an absorption of the RF cavity. Furthermore, to increase the efficiency of removing the heat from the inside of the crystal, the whole RF cavity is contacted to the Helium4 cooled by the mixing chamber.

The points for realizing the low field are following.

1. Relaxation time of electrons spins at 0.1 K in 0.1 T : From the measurements of the relaxation time of the Al NMR spectrum with the single crystal of LaAlO_3 doped with $0.03\text{ mol}\%$ Nd elements, it has found that the origin of the spin-lattice relaxation of the electron spins is not the direct process as shown in Fig. 14. This implies the independence from the magnetic field. As the results, the relaxation time is $0.5\mu\text{sec}$ in 0.1 T and at 0.1 K , which is sufficiently short for realizing the polarization transfer.
2. Relaxation time of La at 0.1 K in 0.1 T : The estimation of the relaxation time of La from the measurements with the identified crystals is indicated

in Fig. 15. From the results, the relaxation time at 0.1K in 0.1T is estimated to 40 min. The longer relaxation time can be expected by improve the quality of the crystals and decrease amounts of the impurities.

3. Q value of the RF cavity : In order to perform the ISE, the frequency should be swept during about 20MHz, which is corresponds to the ESR linewidth of 6G, which is known from the previous measurements. The resonant frequency of the RF cavity is 2.8GHz, so that the corresponding Q value is about 150. Since the crystal of LaAlO_3 is generally used as the ferroelectric substrate for the microwave, the RF loss due to the crystal is not so much. Therefore, the Q value of 150 including the crystal is fully possible.

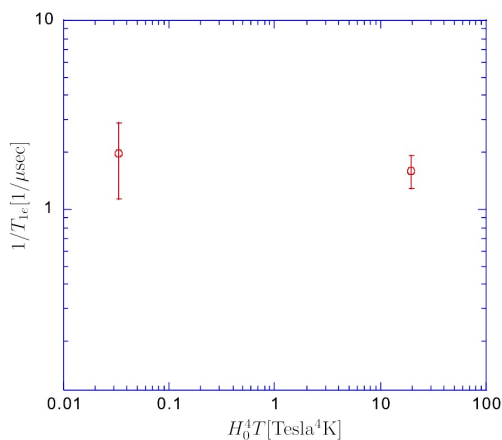


FIG. 14: Results of T_1 of Nd ions in LaAlO_3

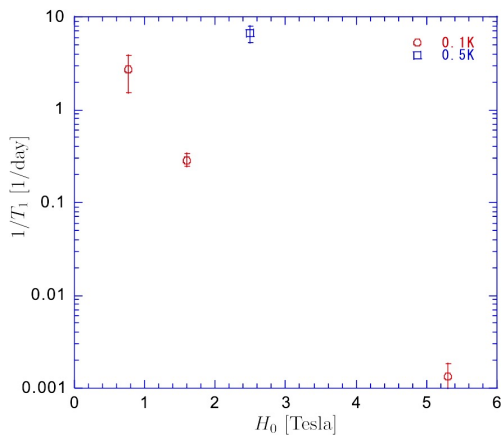


FIG. 15: Results of T_1 of La in LaAlO_3 , which can be obtained by converting from the Al NMR

From the above arguments, the low field DNP at 0.1K in 0.1T is practically possible. The Helmholtz magnet,

the superconducting shield, the RF cavity, 4K dewar, 0.1K dilution are essential elements for developments.

1. R&D items and requirement

As shown in Fig. 16, the 0.1 dilution, which includes the RF cavity, is inserted in the Helmholtz magnet mounted inside of 4K Helium dewar. The design of the

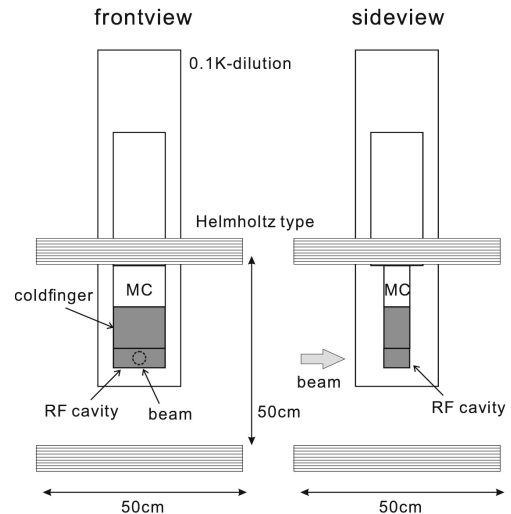


FIG. 16: Structure of the Helmholtz magnet and the 0.1K dilution. The RF cavity inside of the 0.1K dilution is cooled down by the cold finger and Helium4.

Helmholtz magnet which produces the magnetic field of 0.1T and the homogeneity of 10^{-4} is not practically difficult. But, it is not easy to keep the strength of the magnetic field constant inside of the superconducting shield. If necessary, we also consider the combination with shim coils. The development of the magnet fulfilling the demand from the systematics is necessary.

The design of the RF cavity is shown in Fig. 17 The crystal is cooled down via the RF cavity, which is cooled down with the thermal contact to the cold finger. In the TE102 mode, the oscillating magnetic field is perpendicular to the applied magnetic field, but the maximum is at the center and the minimum is at 2.5 cm far from the center.

On the crystal growth, the fundamental studies for small high-quality crystals are proceeding in the Institute of Material Research(IMR), Tohoku University and the basic parameters for a Floating Zone method has been already clarified. The remaining issues are to control the structure of twin domains and to make it more bigger.

The requirements of the cryogenics are summarized as below.

- 4K dewar : cylindrical structure, which dimension is the diameter of 130cm and the height of about 110cm.

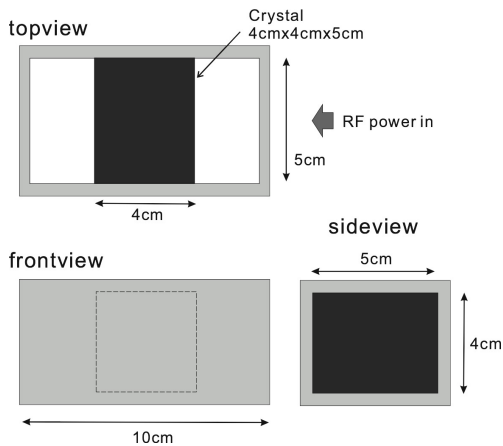


FIG. 17: Design of the RF cavity and the target crystal. The RF cavity is rectangular, made of copper and has the TE₁₀₂ mode.

- Magnet and magnetic shield : The developments of the magnet which holds the magnetic field constant, and the superconducting shields which are isolated from the outside are necessary.
- 0.1K dilution : The RF cavity which dimension is 10cm × 5cm × 5cm is mounded and cooled down by the cold finger and Helium4. The heat load of 1mW is required at 0.1K.
- RF irradiation system : The RF source with the frequency of 2.8GHz, the power of several hundred mW, and the function of the frequency sweep of 20MHz is necessary. To make the RF pulse, the RF switch is needed.

B. Third option: Brute force

If the crystal is left under the condition of 17T and 0.01K, the La thermal polarization of 50% can be obtained. In the Research Center of Nuclear Physics (RCNP), such cryogenics system is still working. The polarization is growing up to 50 % by just putting the crystal in the target station. After obtaining the enough polarization, the crystal is carried to J-PARC with keeping the highly polarization and slowly installed in the target cryostat, where the magnetic field of 0.1T is applied and the magnetic shield is started up. Therefore, the magnet and the superconducting shields in the 4K dewar is the same as the ones in the low field DNP. But, the design of the 0.1K dilution is changed as shown in Fig. 18. The polarized target is transferred to the portable cryostat, which produces the condition of 1.5K and 1.5T and is provided by RCNP, carried to the J-PARC, and transferred again into the 0.1K dilution through the insert rod. In the brute force, the crystal doped with Nd elements is unnecessary. The relaxation time in the pure

crystal of LaAlO₃ is significant. Unfortunately, it is too long and has not been measured yet at the low temperature. Hence, the exact relaxation time is unknown.

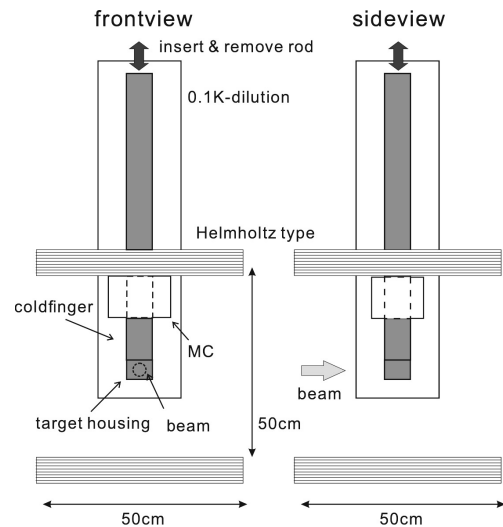


FIG. 18: Structure of the Helmholtz magnet and the 0.1K dilution in the polarized target obtained by the brute force. The rod supporting the crystal housing can be inserted in and removed from the 0.1K dilution

1. R&D items and requirement

The 0.1K dilution with the similar function is commercially available. Additionally, we need two cryostats for transferring the crystal from the target station to the portable cryostat and from the portable one to the cryostat in the beamline. Two cryostats for the transfer are also commercially available. The significant issues are similar to the case in the low field DNP. The developments of the 4K dewar, the magnet, and the magnetic shield are necessary.

C. Present Status

The current status of R&D items without polarized target are described below.

1. Studies of Nuclear Reactions

This experiment is based on the framework of compound nuclei with the mixing of s- and p-wave components. Before all, and at the same time, the details of nuclear reaction must be studied.

In order to estimate the possibility of the candidates as the target, we have measured the κ value of ^{139}La by observing of (n, γ) reaction. According to the s-p mixing formalism, the angular distribution of emitted γ -ray from a resonance state can be explained by using the relative amplitude of each partial wave component. At the p-wave resonance neighboring the large s-wave peak, only the ratio between $j = 1/2$ and $j = 3/2$ in the p-wave component is an unknown parameter. The angular distribution of γ -ray appears even when both of the neutron and the target are not polarized.

We have successfully measured the angular distribution from $^{139}\text{La}(n, \gamma)$ reaction at BL04 ANNRI beamline in MLF at J-PARC. The germanium γ -ray detectors with high resolution of γ -ray energy and the time-of-flight measurement of pulsed neutrons to resolve the neutron energy enabled us to determine the final state of the reaction and to extract the γ -ray distribution. The observed distribution was explained by using the s-p mixing formalism. Finally we get the finite region of the κ parameter, which have the magnitude of the order of 1. This showed that ^{139}La is the promising candidate for the T-violation search experiment because the enhancement of T-violating process is about 10^6 .

By using polarized neutron beam, we can study more details of the nuclear reaction, for example, the validity of the s-p mixing formalism. We have already tried to install the neutron polarizer based on ^3He spin filter into the ANNRI beamline. Although the polarization was about 20%, we measured some correlation terms of the γ -ray. The longitudinal asymmetry, which represents P-violation and connects to C term, was observed. It was consistent with the literature values of previous measurements. We have also measured the transversal asymmetry (a correlation term with $(\sigma_n \cdot (\hat{k}_n \times \hat{k}_\gamma))$). The results are ready to publish.

In order to search the other candidates of the target nuclei, we are continuing the measurement of (n, γ) reactions at ANNRI beamline. For example, ^{117}Sn is one of the candidates because it has the nuclear spin of $1/2$, which the description of the forward scattering amplitude can be written very simply. Even though ^{131}Xe is a gas in room temperature, there is a possibility to polarize the Xe nuclei by using optical pumping method.

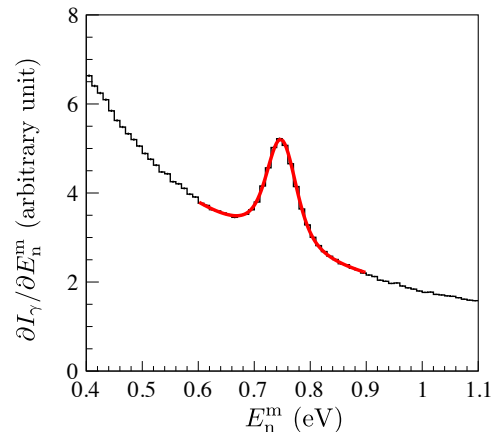


FIG. 19: Resonance peak fit of La

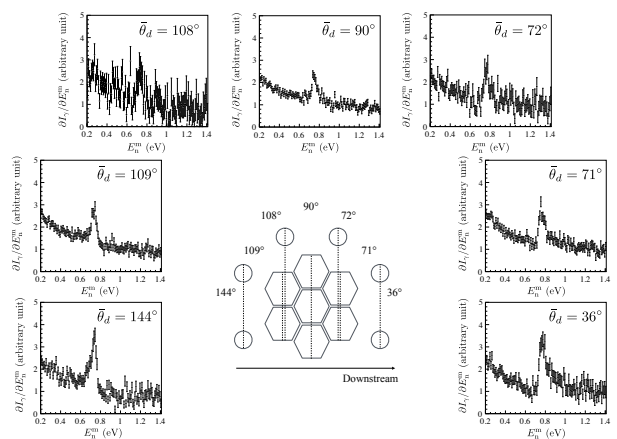


FIG. 20: Gamma-ray asymmetry of La

2. ^3He Spin Filter

The development of the ^3He spin filter is mainly conducted at J-PARC and KEK. A gas filling station for ^3He spin filters are constructed at J-PARC in last year. We fabricated several ^3He spin filters using pure Rb and Rb and K, and a long relaxation time of the ^3He polarization with around 200 h is achieved for four ^3He spin filters by improvement of a rinse process of the glass cell. A ^3He spin filter with ^3He thickness of 29.3 atm-cm and radius of 6.5 cm is now available (Fig. 22). Therefore, the ^3He spin filter with 79 atm-cm can be achieved by using series of the two or three ^3He spin filters.

Currently, we are developing a fiber laser system with 110 W which can irradiate the laser light from both sides of a ^3He spin filter and can be installed neutron beam lines (Fig 23). The ^3He polarization of over 70% has been achieved by using this laser system with the hybrid cell of 21 atm-cm ($\phi 4.5 \text{ cm} \times 7.5 \text{ cm}$). As an SEOP system using 200 W laser has been reported in Oak Ridge National

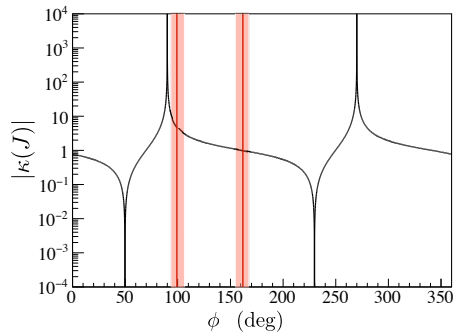


FIG. 21: κ value of La



FIG. 22: A ^3He spin filter with a dimension of $\phi 6.5$ cm and 11.5 cm.

Laboratory, it seems possible to develop the above laser system.

The development of the proton spin filter to polarize epi-thermal neutrons are also ongoing at RIKEN. The proton is polarized by the triplet DNP. They made a large crystal of $\phi 15 \times 4$ mm, and 28 % of the proton polarization was achieved at 90 K. They conducted an experiment to polarize neutron beam with RANS (Accelerator-driven compact neutron source at RIKEN) and obtained 8.5% polarization for 1-10 eV neutrons. As 80% proton polarization has been reported at PSI, the proton polarization will be improved by using cryostat with liquid He.

3. Neutron Detector

1. Required detector performance

The detector used in this study is sensitive in the assumed resonance energy region, and an epithermal neutron detector that can be used in the region of approximately 1 eV is required. Assuming a full neutron beam of MLF beamline, it is desirable that the instantaneous count rate in the 1 eV region is about $100\text{Mcps/cm}^2 \sim 1\text{Gcps/cm}^2$. In addition, if estimate from statistics, in order to count about 10^{10} event in 30 days, an instantaneous count rate of 1 Mcps is required. Therefore, the performance

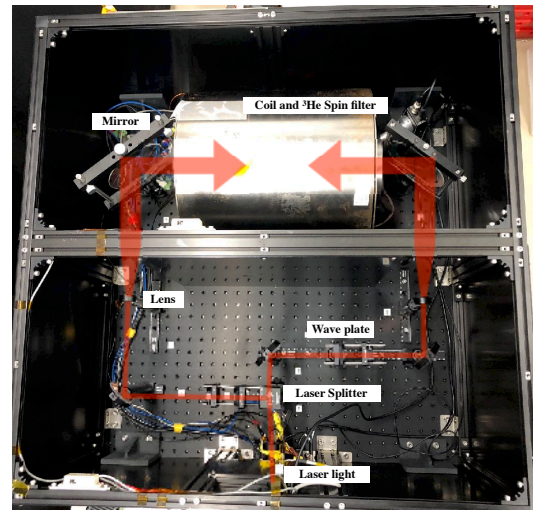


FIG. 23: Laser system which can be install to a neutron beam line to polarize a ^3He spin filter during a neutron experiment.

required for the detector is at least 1 Mcps, and if possible, a neutron detector that satisfies 1 Gcps is required.

There are no fast neutron detector satisfying such an instantaneous count rate has been realized, so the following two types of detector candidates are planned and developed.

- (a) Current mode operation of PMT output by detecting γ rays with using ^{10}B neutron converter.
- (b) Development of a new high count rate neutron detector using scintillators with a short decay time constant

Currently, Kentucky University is proceeding with the design and production of 1. as the candidate detector for this research project, and the Japanese side is proceeding with the study of 2. as the backup detector.

2. Current mode detector

It is desirable that the detection efficiency is as high as possible since the measurement requires many statistics. On the other hand, the maximum instantaneous counting rate of the neutron is about $2 \times 10^8 \text{n/s/cm}^2$ in the $E_n = 1\text{eV}$ region. In such a high count rate measurement, the output signal may be continuous even when a detection element and an amplifier with a fast time constant are used. The first candidate of our transmission neutron detector is the Current Mode Detector, which is a method of reading the current of PMT output signal. Figure 24 shows the schematic view of the our Current Mode Detector, which is developed at Kentucky University. Incident neutron beam is stopped

at ^{10}B converter plate and converted to 0.388 MeV γ rays. The γ rays are detected with a nearby NaI detector. The detector test is progressing at J-PARC MLF BL10 and Los Alamos Neutron Science Center.

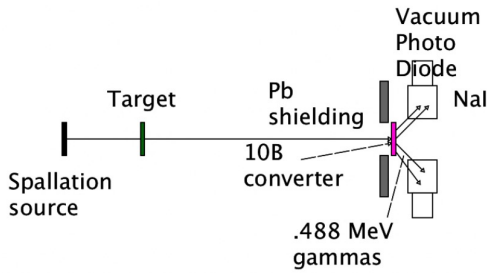


FIG. 24: Current mode neutron detector

3. Scintillation detector

In order to achieve high counting rate by photon counting the epithermal neutrons with a scintillation detector, it is required to have a fast decay time, a solid that can be segmented, and a time characteristic that allows n/γ discrimination. Liquid scintillator containing the ^{10}B has been commonly used to detect neutrons in eV region and the candidate. The decay time of this liquid scintillator is about 4ns, very high counting rates can be achieved using this scintillator. Moreover, since γ -rays can be background for the measurement, neutron and γ -ray discrimination is also important. The discrimination can be performed by using the pulse shape difference between the neutron and the γ -ray detection. On the other hand, since the material is liquid, it is difficult to segment and it is difficult to increase the counting rate of the whole detector.

The other candidate is the ^{10}B containing plastic scintillator, and CsI(pure) scintillator with B layer. Both scintillator has the decay time of about 10 ns. Both are solid and can be segmented. The plastic scintillator is not available the n/γ separation but there is a possibility that detection efficiency can be increased. The CsI(pure) scintillator with B layer detector may be available n/γ separation. The evaluation of these scintillators are proceeding.

A scintillator with a large light yields causes a voltage drop in the PMT in high count measurement, so it is better to use a scintillator with a small light yield.

IV. RESOURCES AND REQUESTS

Human resources

	(FTE)	Responsibility
Beamline design	1	(K. Mishima (KEK))
Neutron polarizer	1	(T. Ino (KEK), T Oku (J-PARC))
Polarized target	3	(M. Inuma (Hiroshima U.))
Neutron detector	1	(B. Praster (Kentucky U.))

Technical or facility resources

- Liquid He supplying facility for development of polarized target (KEK)
- Dedicated epithermal neutron beamline (J-PARC MLF)

Budget

	Amount (kJPY)
Beamline construction	420,000
Neutron polarizer	39,000
Polarized target	325,000
Gamma-ray detector	232,000
Neutron detector	230,000

A. Epithermal neutron beamline

In order to study the compound nuclear reactions by using transmitted neutrons and/or (n, γ) reactions, new neutron beamline which can derive epithermal neutrons must be constructed. Currently we are carrying out the basic research at BL04 ANNRI beamline in J-PARC, however, the the advanced studies of compound nuclei requires much longer beamtime, which can not be supported at the general-use beamtime. The existing beamline does not have sufficient space to install the in-situ neutron polarizer, analyzer, and polarized target system. Especially the polarized target system requires long-term occupation of beamline for in-beam developments.

It contains a neutron collimator and a disk chopper system to optimize the beam cross section and energy spectrum at the target position. Radiation shields for neutrons and γ -rays are required to allow scattering in epithermal region and consequently they will be the similar scale of structure of BL10 (NOBORU). We estimate two full-time equivalent researchers for the detailed design and construction of the beamline in the first year of this project.

TABLE II: Epithermal neutron beamline

Item	Amount (kJPY)
Radiation shield	300,000
Neutron beam guide	100,000
Disk chopper	10,000
Electricity facility	10,000

B. Neutron polarization system

As a first candidate of a neutron polarizer, ^3He spin filter is now developed for epithermal neutrons. For p-wave resonance of ^{139}La , neutrons with the energy of 0.75 eV must be polarized. It requires 60 atm cm ^3He gas with a large cell. High power laser with narrow bandwidth to polarize Rb atom for SEOP pumping. In-situ spin filter system will be install into the neutron beamline for stable operation. Monitoring NMR signals of ^3He is used.

One full-time equivalents researchers make effort for development of the neutron polarizer in the first year of this project, and he will support the stable operation of the polarizer in the experiments.

TABLE III: Neutron polarization system

Item	Description	Unit	Amount (kJPY)
^3He gas cell		10	2,000
^3He gas	10 litter	1	3,000
Gas filling system		1	4,000
Laser system	laser, optics	2	24,000
NMR+EPR system		2	6,000

C. Polarized target system

Polarized nuclear target is necessary in the beamline. Present top-priority candidate for T-violation search is ^{139}La .

The actual target material is LaAlO_3 single crystal with the size of 4 cm \times 4 cm \times 6 cm. First of all, large size of the single crystal needs to be grown.

We are planning to apply the dynamic nuclear polarization (DNP) technique in low magnetic field of 0.1 T so that the DNP can be applied through the T-violation measurement under the pseudomagnetism-compensation. The successful demonstration of DNP of lanthanum nuclei with 2.3 T magnetic field needs to be extended to the low magnetic field environment by developing a refrigerator at the operation temperature of around 0.1 K with a sufficient cooling power to accept the continuous microwave irradiation.

The magnetic field distribution needs to be uniform at the level of 10^{-4} or better for DNP. Additionally, non-adiabatic boundary condition of magnetic field is

preferred to accept divergent beam for better statistics, which requires sharp edge of the target material, superconducting magnetic shield with sufficient shape precision at low temperatures.

For the development of polarized target, we estimate that three full-time equivalents researchers are necessary for three years.

TABLE IV: Polarized target system

Item	Description	Amount (kJPY)
Dilution refrigerator	Vacuum pump, ^3He	150,000
Superconducting magnet	0.1 T	100,000
Microwave source	2.8 GHz	50,000
NMR system		5,000
Sample preparation	target crystal	20,000

D. Gamma-ray and neutron detector system

Both neutron and gamma rays detecting system are must be set on the beamline. The neutron detector is mainly used as the transmission detector, which need high counting rate. The gamma-ray detector are using for the (n, γ) reaction measurement. The Ge detector are also using for the identify the final state(F) of the compound nucleus. The neutron transmission detector, which is incident neutron beam monitor, and scattering neutron detector also must be set at beamline.

TABLE V: Gamma-ray detector system

Item	Unit	Amount (kJPY)
Ge detector	20	200,000
BGO detector	2	4,000
Detector mount system	1	4,000
Gamma-ray collimator	1	4,000
Gamma-ray shield	1	4,000
DAQ system (20 channels)	1	20,000

TABLE VI: Neutron detector system

Item	Unit	Amount (kJPY)
High counting rate Neutron detector	20	50,000
Transmission detector (beam monitor)	1	10,000
scattering neutron detector	1	30,000
Detector mount system	1	4,000
collimator	1	4,000
Gamma-ray and neutron shield	1	4,000
DAQ system (20 channels)	1	20,000

E. Schedule

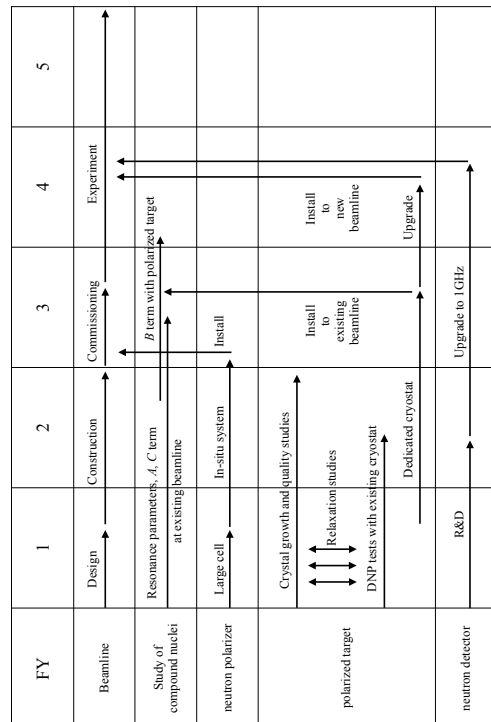


FIG. 25: Schedule

-
- [1] A. D. Sakharov, *Pisma Zh. Eksp. Teor. Fiz.* **5**, 32 (1967).
 - [2] G. E. Mitchell, J. D. Bowman, and H. A. Weidenmuller, *Rev. Mod. Phys.* **71**, 445 (1999).
 - [3] G. E. Mitchell, J. D. Bowman, S. I. Penttila, and E. I. Sharapov, *Phys. Rep.* **354**, 157 (2001).
 - [4] V. G. Baryshevsky and M. I. Podgoretsky, *Zh. Eksp. Teor. Fiz.* **47**, 1050 (1964).
 - [5] V. P. Gudkov, *Phys. Rev.* **C46**, 357 (1992).
 - [6] V. Gudkov and H. Shimizu, *Phys. Rev. C* **95**, 045501 (2017).
 - [7] V. Gudkov and H. Shimizu, *Phys. Rev. C* **97**, 065502 (2018).
 - [8] V. Gudkov and H. Shimizu, arXiv:1910.08598.
 - [9] G.E. Mitchell, J.D. Bowman, S.I. Penttilä and E.I. Sharapov, *Physics Reports*, **354** 157 (2001).
 - [10] V. V. Flambaum and O. P. Sushkov, *Nucl. Phys. A* **435**, 352 (1985).
 - [11] T. Okudaira *et al.*, *Phys. Rev. C* **97**, 034622 (2018).
 - [12] P. Hautle and M. Iinuma, *Nucl. Inst. Meth. Phys. Res. A* Vol. **440** 638 (2000).
 - [13] Y.H.Song, R. Lazauskas, and V. Gudkov. *Phys. Rev. C* **83** 065503 (2011).
 - [14] S. F. Mughabghab. *Atlas of Neutron Resonances* 5th ed. Elsevier, Amsterdam, 2006.
 - [15] Pavel Fadeev and Victor V. Flambaum, *Phys. Rev. C* **100**, 015504 (2019).
 - [16] D. Blyth *et al.*, *Phys. Rev. Lett.* **121**, 242002 (2018).
 - [17] P, K. Kabir, *Phys. Rev. D* **37**, 1856 (1988).

Collaboration List

Hirohiko M. SHIMIZU	Nagoya Univ. PI
W.M. SNOW	Indiana Univ. US team leader

Beamline

Kenji SAKAI	JAEA
Kenji MISHIMA	IMSS, KEK

Neutron Polarizer

Takayuki OKU	JAEA
Takuya OKUDAIRA	JAEA
Takashi INO	IMSS, KEK
Tomohiro UESAKA	RIKEN
Ken'ichi TATEISHI	RIKEN
Hiroki IKEGAMI	RIKEN

Neutron spin control

Masaaki KITAGUCHI	Nagoya Univ.
-------------------	--------------

Nuclear polarization

Masataka IINUMA	Hiroshima Univ.
Taku MATSUSHITA	Nagoya Univ.
Nobuo WADA	Nagoya Univ.
Shigeru ISHIMOTO	IPNS, KEK
Hideki KOHRI	RCNP, Osaka Univ.
Masaru YOSOI	RCNP, Osaka Univ.
Takahiro IWATA	Yamagata Univ.
Yoshiyuki MIYACHI	Yamagata Univ.
Daisuke TAKAHASHI	Ashikaga Univ.
Ryosuke ISHIGURO	Japan Women's Univ.
P.Hautle	Paul Scherrer Institut
Takamasa MOMOSE	Univ. British Columbia

Target material

Masaki FUJITA	IMR, Tohoku Univ.
---------------	-------------------

Neutron detector

W.M. SNOW	Indiana Univ.
J. CUROLE	Indiana Univ.
J. CARINI	Indiana Univ.
B. PLASTER	Kentucky Univ.
D. SCHAPER	Kentucky Univ.
C. CRAWFORD	Kentucky Univ.
B.M. GOODSON	Southern Illinois Univ.
A.S. TREMSIN	Univ. California Berkeley
M. VEILLETTE	Berea College
Katsuya HIROTA	Nagoya Univ.
Tatsushi SHIMA	RCNP, Osaka Univ.

Simulation

Tamaki YOSHIOKA	Kyushu Univ.
-----------------	--------------

Theory

V. GUDKOV	Univ. South Carolina
Kazuyuki OGATA	RCNP, Osaka Univ.
Koichi HAGINO	Kyoto Univ.
Junji HISANO	Nagoya Univ.

General

Hiroyuki FUJIOKA	Tokyo Inst. Tech.
Atsushi Kimura	JAEA
Shunsuke ENDOH	JAEA
Hideo Harada	JAEA
K.Taketani	IMSS, KEK
Go Ichikawa	IMSS, KEK
Yutaka Yamagata	RIKEN
Yoshiro I. Takahashi	Kyoto Univ.
Masahiro Hino	Kyoto Univ.
G.N.Kim	Kyungpook Univ.
S.W.Lee	Kyungpook Univ.
H.J.Kim	Kyungpook Univ.
J.D.Bowman	Oak Ridge National Lab.
S.Penttila	Oak Ridge National Lab.
X.Tong	Oak Ridge National Lab.
P.Jiang	Oak Ridge National Lab.
Yoshiro KIYANAGI	Nagoya Univ.
Takahiro MORISHIMA	Nagoya Univ.

Appendix A: Coefficients in the Forward Scattering Amplitude

The explicit expressions of the coefficients in Eq. 5 for the case of ^{139}La ($I=7/2$) are described below [8].

$$\begin{aligned}
A' &= \frac{1}{16}(7a_{s0} + 9a_{s1}) + \frac{9}{32} \frac{i}{k_n} \left(\mathcal{W}_{s0} + \mathcal{W}_p + \frac{7}{9} \mathcal{W}_{s1} \right) \\
B' &= \frac{\sqrt{21}}{16}(a_{s0} - a_{s1}) + \frac{\sqrt{21}}{32} \frac{i}{k_n} \left(\mathcal{W}_{s0} - \mathcal{W}_{s1} \right. \\
&\quad \left. + \mathcal{W}_p \left(-\frac{39}{28} x_S^2 + \frac{9}{2\sqrt{35}} x_S y_S + \frac{9}{20} y_S^2 \right) \right) \\
C' &= \frac{9}{16} x \frac{v}{\sqrt{\Gamma_{s0}^n} \sqrt{\Gamma_p^n}} \frac{1}{k_n} \mathcal{W}_{s0} \mathcal{W}_p \\
D' &= -\frac{2}{3} \frac{w}{v} \frac{x_S}{x} C' \\
H' &= -\sqrt{3} \frac{1}{x} \left(\frac{1}{6} x_S + \frac{\sqrt{35}}{6} y_S \right) C' \\
K' &= \frac{3}{128} \sqrt{\frac{3}{7}} \left(3x_S^2 + 18\sqrt{\frac{7}{5}} x_S y_S + \frac{77}{5} y_S^2 \right) \frac{i}{k_n} \mathcal{W}_p \\
E' &= -\frac{9}{256} \sqrt{\frac{3}{7}} \left(5x_S^2 + 6\sqrt{\frac{7}{5}} x_S y_S + \frac{77}{5} y_S^2 \right) \frac{i}{k_n} \mathcal{W}_p \\
F' &= \sqrt{\frac{3}{5}} \frac{y}{x} C' \\
G' &= -\frac{9}{32} \sqrt{\frac{3}{5}} (x_S y'_S - x'_S y_S) \frac{i}{k_n} \frac{v_T^{pp'}}{\sqrt{\Gamma_p^n} \sqrt{\Gamma_p^n}} \\
B'_3 &= -\frac{81\sqrt{33}}{2240} y^2 \frac{i}{k_n} \mathcal{W}_p, \tag{A1}
\end{aligned}$$

where k_n is neutron momentum, a_0 and a_1 are the scattering length of ^{139}La for $J = 4$ and $J = 3$ respectively, x and y are $j = 1/2$ and $j = 3/2$ contribution in the p-wave resonance respectively, x_S and y_S are channel spin $S = I - 1/2$ and $S = I + 1/2$ respectively. And \mathcal{W}_{s0} , \mathcal{W}_{s1} , \mathcal{W}_p are Breit-Wigner amplitude formula for the negative, p-wave at 0.75 eV, and s-wave at 72eV resonances respectively, Γ_{s0}^n , Γ_p^n , Γ_{s1}^n are neutron width of the Brite-Wigner parametrization:

$$-i\mathcal{W}_r = \frac{\Gamma_r^n}{E - E_r + i\Gamma_r}, \tag{A2}$$

where E is neutron energy, E_r is resonance energy, and Γ_r is total width of the resonance r.

Here we summarize the method to determine each coefficients.

A'

The A' term can be measured by using unpolarized neutrons and unpolarized target. The precision of the resonance parameter, including the negative resonance, is quite important for all studied. We should perform the A' measurement even if we use the conventional beamline in J-PARC. It can be done at BL04 ANNRI for the early time, and we will shift the activities to the our own newer beamline.

B'

The B' term is related to pseudomagnetic field by polarized target. Once the polarized target is available, we start to study the B' and related terms. Especially the energy dependence of the B' term is important issue, which was not demonstrated in previous experiments. We can measure that by using TOF mentioned in the section about measurement principle.

C'

The C' term is parity violating amplitude between neutron spin of $+z$ and $-z$. The C' term is independent from the nuclear polarization I . The study of C' term can be started even if the polarized target is not available. The C' term makes the largest false asymmetry in $\text{Re}A^*D$ measurement. The accuracy can be same as the D' term because the same order of magnitude of the measurement time can be used while $\text{Re}A^*D$ measurement.

H' and E'

The H' and E' term is the effects from $(k_n \cdot I)$. The H' is related to target vector polarization P_1 and the E' is related to target tensor polarization P_2 . Because theses are not related to neutron spin, the effects are eliminated in the asymmetry calculation in principle.

K'

The K' is the effects from $P_1(\sigma_n \cdot k_n)(k_n \cdot I)$. After the polarized target is available, the measurement of K' can start. The magnitude of K' is the same as the order of C' , however, the neutron-energy dependence is different from that of C' . The K' effect appears only near around p-wave resonance peak. We can extract the K' effect by fitting of the TOF data with K' effect (only the p-wave resonance shape) and the other terms effects which have the shape of the interference between s- and p-wave resonances. The neutron momentum direction can be controlled in order to suppress and estimate the K' effect. The $(\sigma_n \cdot k_n)$ can be change

by controlling beam direction k_n . The neutron slits just before the target can be scanned to control the beam direction, for example.

F'

The F' is the effects from $P_2(\sigma_n \cdot I)(k_n \cdot I)$ and $P_2(\sigma_n \cdot k_n)/3$. The energy dependence is the same as C' and D' , therefore this effect can not be separated by using TOF measurements. And the magnitude of F' is the same as the order of C' . The F' can be extracted by comparing the P-violation between the polarized and unpolarized target.

G'

The G' is the effects from the interference between the p-wave resonance, which we are focusing at 0.75 eV, and the other p-wave resonance. In this paper, we neglect this effect because there is no p-wave resonance peak with sufficient amplitude near around

the 0.75 eV peak.

B'_3

The B'_3 is the effects from $P_3(\sigma_n \cdot I)((k_n \cdot I)^2 - 1)$ and $P_3(\sigma_n \cdot k_n)(k_n \cdot I) \times (2/3)$.

The magnitude of B'_3 is the same as the order of C' , however, the neutron-energy dependence is different from that of C' . The B'_3 effect appears only near around p-wave resonance peak. We can extract the B'_3 effect by fitting of the TOF data with the same procedure of K' extraction (or we extract the information of the integration of K' and B'_3).

As discussed above, the contaminations from all coefficients can be extracted and/or estimated with the accuracy same as D' term. The neutron polarization σ_n and the target polarization are monitored by using NMR technique while measurement.